



# Crack Growth Model for Evaluation the Fatigue Life of Aluminum Alloys

Zahraa M. Chalooob<sup>1\*</sup>, Saad T. Faris<sup>2</sup>, Hussien J.M. Al Alkawi<sup>2</sup> and Ali H. Mohamed<sup>3</sup>

<sup>1</sup>Department of Mechanical Engineering, University of Diyala, 32001 Diyala, Iraq

<sup>2</sup>Department of Aeronautical Techniques Engineering, Bilad Alrafidain University College Diyala, Iraq

<sup>3</sup>Department of Mechanical Technologies, Baquba Technical Institute, Middel Technical University (MTU), Baghdad, Iraq

## ARTICLE INFO

### Article history:

Received June 21, 2023  
Revised October 6, 2023  
Accepted October 10, 2023  
Available December 15, 2023

### Keywords:

AA2014  
AA7075-T651  
Crack growth rate  
Replication technique  
Short and long cracks

## ABSTRACT

The main objective of this study is to experimentally determine the fatigue life of the aluminum alloys AA2014 and AA7075-T651 by measuring the lengths of short and long cracks practically under bending stress with constant amplitude loading and stress ratio ( $R = -1$ ) at room temperature (RT) 25 C0 by employing Basquin's equation. To determine the fatigue life curve for both alloys at five different levels of constant amplitude stresses, the average failure cycles of three specimens at each stress level were recorded. The surface of specimen was replicated with cellulose paper and liquid acetone. This piece was examined using an optical microscope to record the length of the crack and the number of cycles corresponding to it at a constant stress level. The lengths of the cracks were then measured using the replication approach. A unique mathematical model was created to describe the relationship between crack speed ( $da/dN$ ) and the length of short and long cracks in order to predict the overall fatigue life of each alloy. When the model's result was contrasted with actual outcomes, the conclusions were reliable and productive.

## 1. Introduction

Aluminium alloys are a widespread, effective material with a long history of successful use in a variety of industries, notably in aircraft, marine, railway, and automotive applications. Because of its flexibility, strength, high durability, and great resistance to corrosion [1,2]. Due to their high strength, aluminium alloys from the series 2XXX and 7XXX are appropriate for use in the production of airplane parts, and throughout the course of their service life, the mechanical components of these alloys are regularly subjected to complicated loadings [3]. One of the most important types of metal damage is fatigue failure. The Parts that fail frequently operate under safe loads.

The internal structure of the material is changed as a result of cumulative damage buildup brought on by periodic loads. This results in the initiation of microcracks, their formation, the macroscopic expansion of cracks, and finally a surprise fracture that might go undetected if not taken into consideration during the design [4,5]. When a material or component breaks as a result of repetitive dynamic cyclic stress, it is said to have experienced fatigue failure. The three steps it typically goes through are called initiation, crack propagation, and the ultimate fracture. These kinds of cracks are further split into three categories. Mechanically and Physically Short Cracks, Microstructurally Short cracks, and long cracks could occur in the microstructure of the material [6].

\* Corresponding author.

E-mail address: [zahra-mohamed@uodiyala.edu.iq](mailto:zahra-mohamed@uodiyala.edu.iq)

DOI: [10.24237/djes.2023.160411](https://doi.org/10.24237/djes.2023.160411)

This work is licensed under a [Creative Commons Attribution 4.0 International License](https://creativecommons.org/licenses/by/4.0/).



An experimental study carried out by Haigen Jian et al in 2017 [7] to explore how fatigue cracks spread in aluminium alloy AA2124 sheets of different thicknesses, specifically 30mm and 55mm. The researchers utilized various analytical techniques, including optical microscopy, scanning electron microscopy (SEM), transmission electron microscopy (TEM), and electron backscatter diffraction (EBSD), to investigate this phenomenon. The outcomes of the investigation demonstrated that the rate of crack propagation was slower in the 30-mm sheet. This was attributed to its smaller grain size compared to the 55-mm sheet. Consequently, the thinner 30mm sheet demonstrated enhanced fatigue properties as a result of these microstructural influences.

In a study by V. Chaves and co-authors in 2019 [8], the outcomes of a series of tests on samples composed of 7075-T6 aluminium alloy are presented. These experiments were carried out using load control with a stress ratio of  $R = -1$ . The samples included circular perforations of varying diameters and were subjected to tension, torsion, and in-phase biaxial loading conditions. Diverse examination methods were employed, encompassing an optical microscope, a scanning electron microscope (SEM), and a non-contact 3D optical profiler. The objective was to comprehend the behaviour of cracks originating from these perforations. The findings revealed that the point of crack initiation was situated in close proximity to the location of maximum principal stress. Moreover, the direction of crack propagation is closely aligned with the direction of maximum principal stress.

The investigation by Abhay K. Singh et al. in 2019 [9] examined how fatigue cracks initiate and propagate in thin-walled tubular specimens made from aluminium alloy AA-7075. This study encompassed a range of loading scenarios, including multi-axial in-phase bending-torsional loads as well as uniaxial loading involving pure bending or torsion. Across all the tests, a single crack consistently initiated on the plane experiencing the highest shear stress, with the exception of the pure torsion test. In cases of pure bending, crack propagation occurred

within a continuously changing mixed-mode loading environment, forming a trajectory reminiscent of an inverted S-shape. Conversely, under combined bending-torsional loading, the progression of the crack demonstrated a distinct pattern: an initial region dominated by mode I crack propagation, followed by a transitional zone for crack behaviour, and ultimately culminating in a phase of pure mode II growth.

The study conducted by Y. Li et al. in 2019 [10] investigates the fatigue behaviour of aluminium alloy AA7075 when subjected to both axial and torsional loads. To achieve this, meticulously polished specimens in the shape of dumbbells were subjected to fully reversed tension-compression and torsional fatigue tests. To analyse the fracture surfaces and monitor the initiation and progression of cracks, scanning electron microscopy (SEM) was employed. The findings revealed that cracks initiated at the surface of the specimens. Particularly, fracture profiles displayed a notably rough texture during tension-compression fatigue. In the case of torsional fatigue, fracture initiation occurred on the surface farthest from the centre of rotation.

The investigation by Bang and Ince in 2019 [11] presented a comprehensive modelling approach that combines the development of small and large cracks. The proposed framework considers multiple factors influencing crack progression, as described in equation (1). By comparing the projected crack propagation rates and fatigue lifetimes with actual datasets for crack growth and fatigue life of AA2024-T3 and AA7075-T561 alloys, the study demonstrated a favourable alignment between the model's predictions and the observed behaviour of these materials. The newly introduced model can be formulated as follows [11]:

$$\frac{da}{dN} = A_1 [\Delta k - \Delta k_{th}]^{a_1} \quad (1)$$

where  $A_1$  and  $a_1$ , represent material constants, while  $da/dN$ ,  $\Delta k$ , and  $\Delta k_{th}$  correspond to the rate of crack growth, the range of stress intensity factor (SIF), and the threshold for crack growth, respectively.

The main goal of this study is to obtain experimentally the fatigue life of the selected alloy by new crack growth model.

## 2. Experimental work

### 2.1 Material selection

In this investigation, aluminium alloys (AA2014 and AA7075-T651) were chosen as the materials of interest for the analysed models. These alloys were specifically selected due to their favourable mechanical characteristics,

resistance to common forms of corrosion, impressive strength-to-weight ratios, and improved malleability, making them extensively applied in the field of aerospace [12], [13]. The chemical composition of the AL alloys (AA2014 and AA7075-T651) underwent analysis at Iraq's Ministry of Industry and Materials, State Company for Inspection and Engineering Rehabilitation (SIER), and was subsequently compared against established standards:

**Table 1:** Chemical analysis for Aluminium Alloys (AA2014 and AA7075-T651) in wt. %

Element Wt. %	Si	Fe	Cu	Mn	Mg	Cr	Zn	Al
<b>Experimental (AA2014)</b>	0.266	0.498	4.63	0.412	0.521	0.0125	0.198	Balance
<b>Standard [14] (AA2014)</b>	0.5-1.2	0.7	3.9-5	0.4-1.2	0.2-0.8	0.10	0.25	Balance
<b>Experimental (AA7075-T651)</b>	0.105	0.246	1.61	0.0475	2.35	0.218	5.67	Balance
<b>Standard [14] (AA7075-T651)</b>	0.4	0.5	1.2-2.0	0.3	2.1-2.9	0.18-0.28	5.1-6.1	Balance

### 2.2 Roughness test

Every tension and fatigue specimen underwent roughness evaluation using a TR220 roughness testing apparatus, as depicted in figure 1 to obtain a smooth surface free of defects and microscopic gaps that help crack growth. This assessment was conducted at the Applied Science Department, University of Technology. The assessed samples for this research exhibit an average roughness ( $R_a$ ) spanning from 0.1 to 0.7  $\mu\text{m}$ , while the maximum roughness ( $R_z$ ) spans from 1.4 to 2.6  $\mu\text{m}$ .

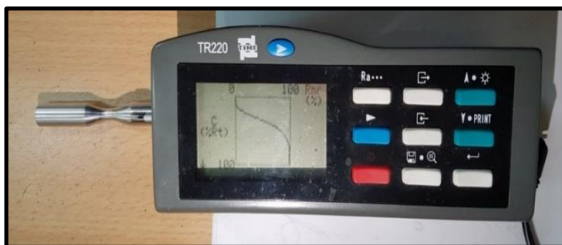


**Figure 1.** portrays the TR220 roughness testing apparatus

### 2.3 Hardness test

Utilizing a Tru-Blue Hardness II Rockwell Hardness Tester, both aluminium alloys (AA2014 and AA7075-T651) underwent a hardness

examination, illustrated in Figure 2, following the ASTM E18 standard to determine the resistance of alloys used to scratching, abrasion or penetration that help to cracks propagation. This testing procedure was conducted at the Iraqi Ministry of Industry and Materials, in collaboration with the State Company for Inspection and Engineering Rehabilitation (SIER).



**Figure 2.** Rockwell hardness tester

## 2.4 Tensile test

The tensile test was conducted at the Iraqi Ministry of Industry and Materials in collaboration with the State Company for Inspection and Engineering Rehabilitation (SIER). The United SHFM Servo-Controlled Hydraulic Tensile Test Machine with a force capacity of 600 KN was utilized to assess the mechanical characteristics of two aluminium alloys (AA2014 and AA7075-T651). The test specimens were prepared following the specifications outlined in the ASTM E8M-16a standard, with their dimensions provided in millimetres, as depicted in Figures 3 and 4.

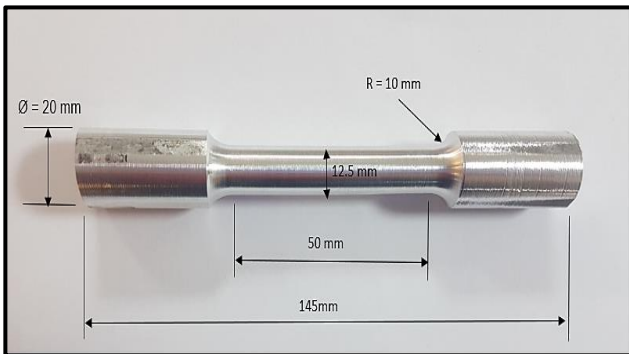


**Figure 3.** Specimen of the tensile test



**Figure 4.** Tensile test machine

## 2.5 Microstructural examination

For each aluminium alloy, a single cylindrical specimen was prepared, featuring dimensions of 15 mm in diameter and 10 mm in length, as depicted in Figure 5. The preparation involved utilizing a lathe to cut the specimens, followed by the use of wet silicon carbide paper with varying grain sizes ranging from 320, 400, 800, and 1200  $\mu\text{m}$  to achieve smoothness. Water served as the cooling fluid during this process. The specimens' surfaces underwent a two-stage polishing procedure. Initially, diamond paste with grain sizes of 6  $\mu\text{m}$  and 2.5  $\mu\text{m}$ , applied to respective cloths, was used. Subsequently, an alumina solution ( $\text{Al}_2\text{O}_3$ ) with a grain size of 0.3  $\mu\text{m}$ , applied to its corresponding cloth, was employed. The polishing was meticulously conducted until all surface scratches were eradicated, rendering the surface akin to a mirror-like finish. This refinement process was facilitated by a Grinder-Polisher apparatus, as illustrated in Figure 6. To enhance visibility and analysis, an etching process was performed on the specimens. The first AA2014 specimen was subjected to an etching solution comprising 25% hydrochloric acid (HCl) and 75% water ( $\text{H}_2\text{O}$ ). Conversely, the second AA7075-T651 specimen underwent etching with a solution composed of 35% HCl and 65% water. Following etching, the specimens were meticulously examined under a microscope with a magnification of 400X. This examination took place within the Baquba Technical Institute's laboratory.

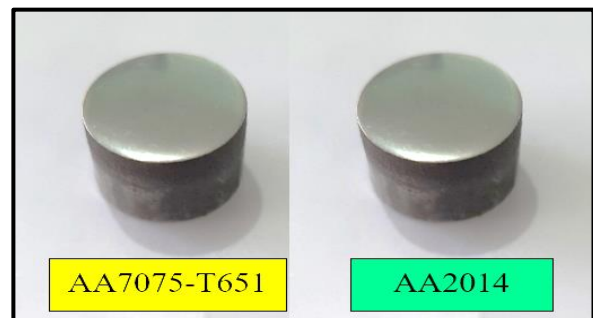


**Figure 5.** Specimens after polishing



**Figure 6.** Grinder-Polisher device

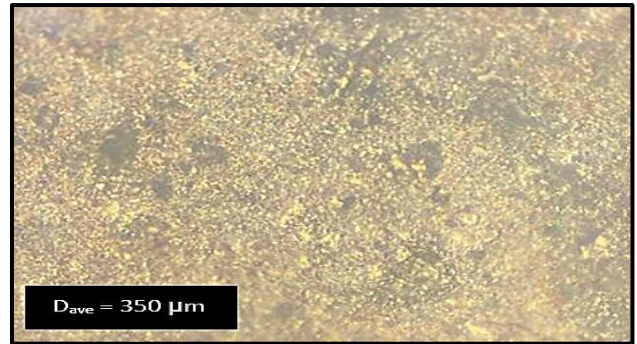


**Figure 8.** Microstructure of AA7075-T651

### 2.6 Average grain size diameter calculation

The linear intercept approach was used to calculate the average grain size diameter for both aluminium alloys, AA2014 and AA7075-T651. This method entailed counting the grains that crossed a predetermined line that was drawn across the 400X magnified microscopic picture on the microscope screen. The average grain diameter was calculated by dividing the micrometre-long length of this line by the number of grains that crossed it. Four measurements were averaged to ensure measurement accuracy. According to the examination, the average grain size for AA7075-T651 is 350 (μm), whereas it is 400 (μm) for AA2014. Figures 7 and 8 show the microstructure of both alloys that used in this process. Equation (3) was used to calculate the average grain size diameter [15].

$$D_{ave} = \frac{W}{L(MG)} \quad (3)$$

where  $D_{ave}$  is the mean diameter of the grain size in μm, while  $W$  stands for the length of the line employed in μm, and  $L$  denotes the count of intersections between the aforementioned line and grain boundaries and  $MG$  represents the magnification factor utilized to visualize the microscopic structure of the specimen.

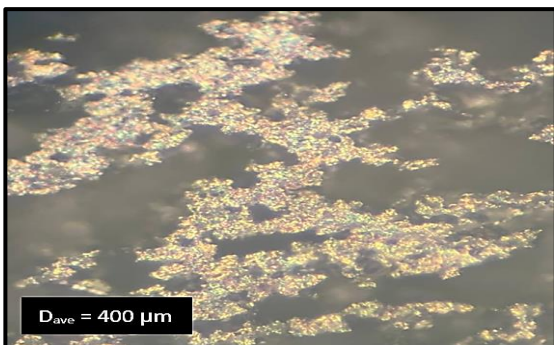


**Figure 7.** Microstructure of AA2014

### 2.7 Fatigue test

All specimens were produced according to the ASTM E466 standard, and all of their measurements are in millimetres. In Fig. 8, the specifications and geometry of the fatigue specimen are shown.

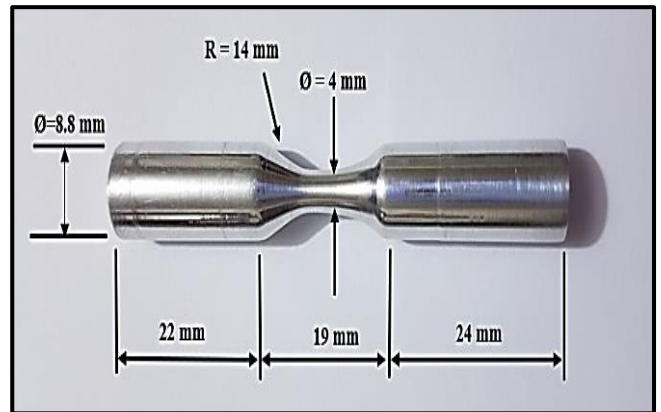


**Figure 9.** The fatigue test specimen

All of the fatigue testing had been done in a lab at the Baquba Technical Institute. The rotating-bending fatigue testing machine of the HI-TECH type was used to test all fatigue specimens with both constant and variable amplitude loading, as shown in Figure 9. The applied load ( $P$ ) is calculated by using the equation (4) as follows [16]:

$$\sigma_B = \frac{32 \cdot P \cdot L}{\pi \cdot d^3} \quad (4)$$

Where  $\sigma_B$  is the bending applied stress and measured in (MPa),  $P$  is the applied load and measured in Newton (N),  $L$  is the arm of the applied load and equals 132 mm, and  $d$  is the minimum diameter of the fatigue specimen and equals 4 mm.

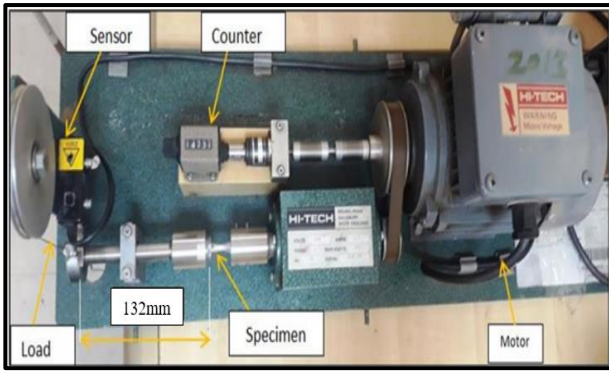


**Figure 10.** Fatigue test machine

## 2.8 Detection of crack growth

The growth of fatigue cracks was tracked using the replication method. Slices of cellulose acetate paper with dimensions of (15 \* 10 \* 0.035 mm) were utilized because they are easy to use and efficient in finding microcracks. The procedure went like this:

Use 3-5 drops of ultra-pure acetone to clean the testing surface, and by using forceps, put the slide on top of the specimen surface, then allow the slide to air dry for a few minutes. The slide is raised and put between two glass slides, also by forceps. The length of the crack was determined by optical microscopy.

## 2.9 Modelling of short and long crack growth

The majority of the equations used in this study are nonlinear, and in order to obtain this kind of power law function, the nonlinear connection's logarithmic values are extracted and transformed into a linear relationship.

### 1- Short Crack modelling

The equation (5) was used to model short cracks whose length is less than the grain's diameter [17]:

$$\frac{da}{dN} = C * (D_{ave} - a_{ave})^\gamma \quad (5)$$

Where C,  $\gamma$  are material constant and  $da/dN$ ,  $D_{ave}$ ,  $a_{ave}$  are the rate of crack speed ( $\mu\text{m}/\text{cycle}$ ), the average grain size diameter ( $\mu\text{m}$ ) and crack length average ( $\mu\text{m}$ ).

To compute the rate of crack speed and average crack length, the equations (6) and (7) are used [17]:

$$\frac{\Delta a}{\Delta N} = \frac{a_{j+1} - a_j}{N_{j+1} - N_j} \quad (6)$$

$$a_{ave} = \frac{a_{j+1} + a_j}{2} \quad (7)$$

Where a, N, and j are the crack length, number of cycles, and scanning number, respectively.

### 2- Long Crack Modeling

The equation (8) shown below was used to model long cracks whose length is greater than the grain's diameter [17]:

$$\frac{da}{dN} = H * (a_{ave})^h \quad (8)$$

Where H and h are constants of material.

## 3. Results and discussions

### 3.1 Tensile test results

To determine the mechanical properties of aluminium alloys AA2014 and AA7075-T651, the results of tensile tests are listed in Table 2. These results were obtained practically using tensile test machine in Figure 4.

**Table 2:** Mechanical properties of AA2014 and AA7075-T651

Condition	UTS (MPa)	YS (MPa)	E (GPa)	Ductility %	Hardness Rockwell HRB
Experimental (AA2014)	524	436	78.5	12.5	67.4
Standard (AA2014) [14]	483	414	72.4	13	67
Experimental (AA7075-T651)	609	590	76.4	11	88.12
Standard (AA7075-T651) [14]	572	503	71.7	11	87

3.2 Fatigue test results

Based on the results mentioned in Table 3, the S-N curve equations were created using the

Basquin power load equation and listed in Table 4. Figures 11 and 12 show the S-N curves of AA2014 and AA7075-T651.

**Table 3:** the results of fatigue test under constant loading of AA2014 and AA7075-T651 with stress ratio R= -1 at room temperature

No. of Spec.	AA2014			No. of Spec.	AA7075-T651		
	Applied Stress (MPa)	N <sub>f</sub> (cycles)	N <sub>f (ave)</sub> (cycles)		Applied Stress (MPa)	N <sub>f</sub> (cycles)	N <sub>f (ave)</sub> (cycles)
1	314 (0.6 UTS)	3500	3600	1	366 (0.6 UTS)	14800	16400
2		4000		2		16900	
3		3300		3		17500	
4	262 (0.5 UTS)	7500	6800	4	305 (0.5 UTS)	68800	64100
5		6100		5		59700	
6		6800		6		63800	
7	244 (0.46 UTS)	10200	10000	7	284 (0.46 UTS)	189400	184100
8		8800		8		179600	
9		11000		9		183300	
10	227 (0.43 UTS)	12300	13000	10	263 (0.43 UTS)	284800	300000
11		12900		11		298900	
12		13800		12		316300	
13	210 (0.4 UTS)	14300	16000	13	244 (0.4 UTS)	417300	412000
14		15700		14		428900	
15		18000		15		389800	

**Table 4:** The S-N curve equations of AA2014 and AA7075-T651[18]

Type of Al Alloy	Equation of S-N curve	R <sup>2</sup> Correlation coefficient	Endurance Limit of Fatigue σ <sub>el</sub> (MPa) at 10 <sup>7</sup> cycles
AA2014	σ <sub>F</sub> = 2623N <sub>f</sub> <sup>-0.259</sup>	R <sup>2</sup> = 0.9936	40.34
AA7075-T651	σ <sub>F</sub> = 1135N <sub>f</sub> <sup>-0.117</sup>	R <sup>2</sup> = 0.9809	172.18

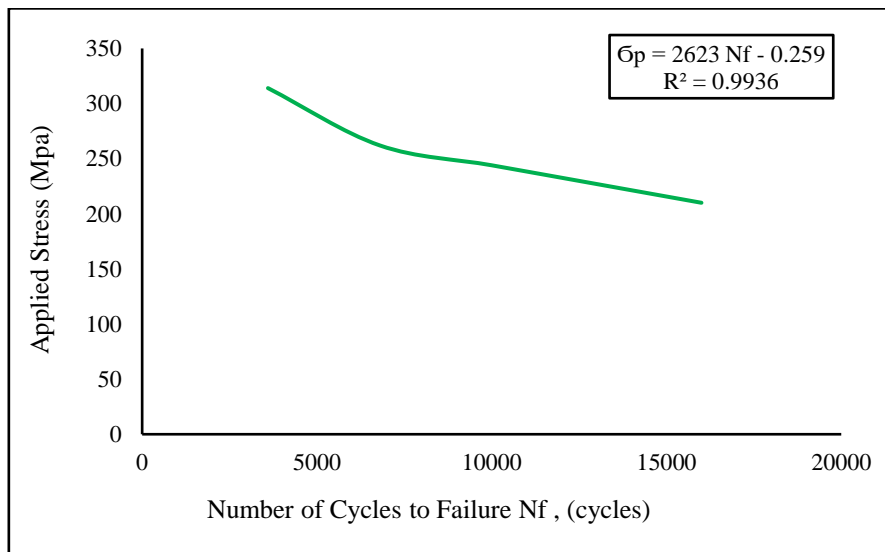


**Figure 11.** S-N curve of AA2014

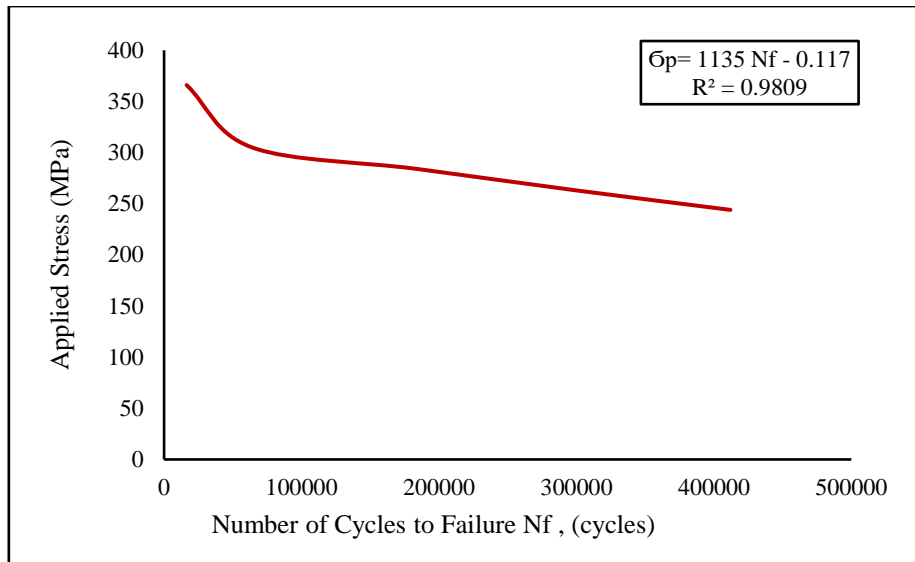


**Figure 12.** S-N curve of AA7075-T651

### 3.3 Detection crack growth results

Figures 13 and 14 show the fatigue cracks path by using an optical microscope. The acetate paper layers of both specimens, it was discovered that the

true crack's path is irregular, running both left and right as it expands toward the small diameter of the fatigue specimen. Figures 13 and 14 depict the two aluminium alloys' fatigue cracks.

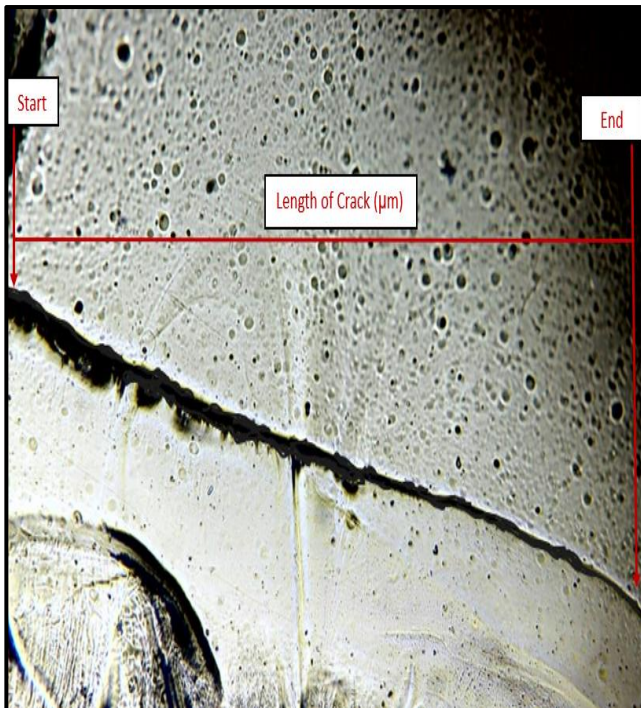


**Figure 13.** The fatigue cracks of AA2014

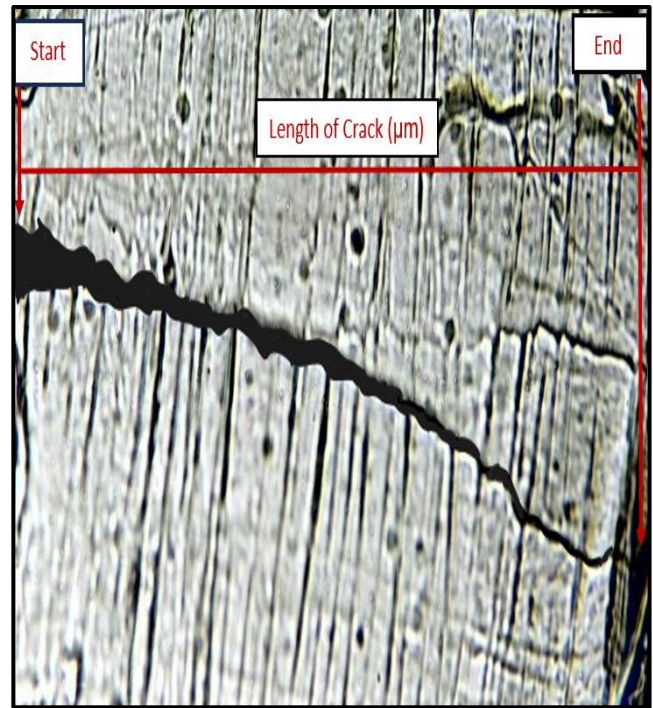


**Figure 14.** The fatigue cracks of AA7075-T651

### 3.4 Results of crack speed measurement

The results of crack speed measurements for the two alloys were listed in Tables 6 and 7.

**Table 6:** The rate of crack speed and crack length average of AA2014 under  $\sigma_F = 105$  (MPa)

No.	a ( $\mu\text{m}$ )	N (cycles)	a <sub>2</sub> – a <sub>1</sub> ( $\mu\text{m}$ )	N <sub>2</sub> – N <sub>1</sub> (cycles)	da/dN ( $\mu\text{m}/\text{cycles}$ )	a <sub>ave</sub> ( $\mu\text{m}$ )	Crack type
1	160	7000	160	7000	0.022857143	80	Short crack
2	210	10500	50	3500	0.014285714	185	Short crack
3	290	12280	80	1780	0.04494382	250	Short crack
4	385	16000	95	3720	0.025537634	337.5	Short crack
5	480	18800	95	2800	0.033928571	432.5	Long crack
6	560	19660	80	860	0.093023256	520	Long crack
7	760	26000	200	6340	0.031545741	660	Long crack
8	950	37000	190	11000	0.017272727	855	Long crack
9	1060	48200	110	11200	0.009821429	1005	Long crack
10	1260	58700	200	10500	0.019047619	1160	Long crack
11	1350	61200	90	2500	0.036	1305	Long crack
12	1460	76000	110	14800	0.007432432	1405	Long crack
13	160	7000	160	7000	0.022857143	80	Long crack

**Table 7:** The rate of crack speed and crack length average of AA7075-T651 under  $\sigma_F = 122$  (MPa)

No.	a ( $\mu\text{m}$ )	N (cycles)	a <sub>2</sub> – a <sub>1</sub> ( $\mu\text{m}$ )	N <sub>2</sub> – N <sub>1</sub> (cycles)	da/dN ( $\mu\text{m}/\text{cycles}$ )	a <sub>ave</sub> ( $\mu\text{m}$ )	Crack type
1	120	70000	120	70000	0.001714286	60	Short crack
2	180	120000	60	50000	0.0012	150	Short crack
3	250	140000	70	20000	0.0035	215	Short crack
4	340	180000	90	40000	0.00225	295	Short crack
5	420	217000	80	37000	0.002162162	380	Long crack
6	610	244000	190	27000	0.007037037	515	Long crack
7	720	315000	110	71000	0.001549296	665	Long crack
8	840	400000	120	85000	0.001411765	780	Long crack
9	970	490000	130	90000	0.001444444	905	Long crack
10	1020	566000	50	76000	0.000657895	995	Long crack
11	1260	625000	240	59000	0.004067797	1140	Long crack
12	1650	885000	390	260000	0.0015	1455	Long crack
13	1810	1000000	160	115000	0.001391304	1730	Long crack

### 3.5 Results of short cracks

The results of these cracks are shown in Table 8. It was determined that small cracks are those

whose average length ( $a_{ave}$ ) is less than the average grain size diameter ( $D_{ave}$ ). Figures 15 and 16 show the short crack behaviour of both alloys.

**Table 8:** The results of short cracks for AA2014 and AA7075-T651

AA7075-T651		AA2014	
$D_{ave} - a_{ave}$	da/dN	$D_{ave} - a_{ave}$	da/dN
290	0.00171428	320	0.0228571
200	0.0012	215	0.0142857
135	0.0035	150	0.0449438
55	0.00225	62.5	0.0255376

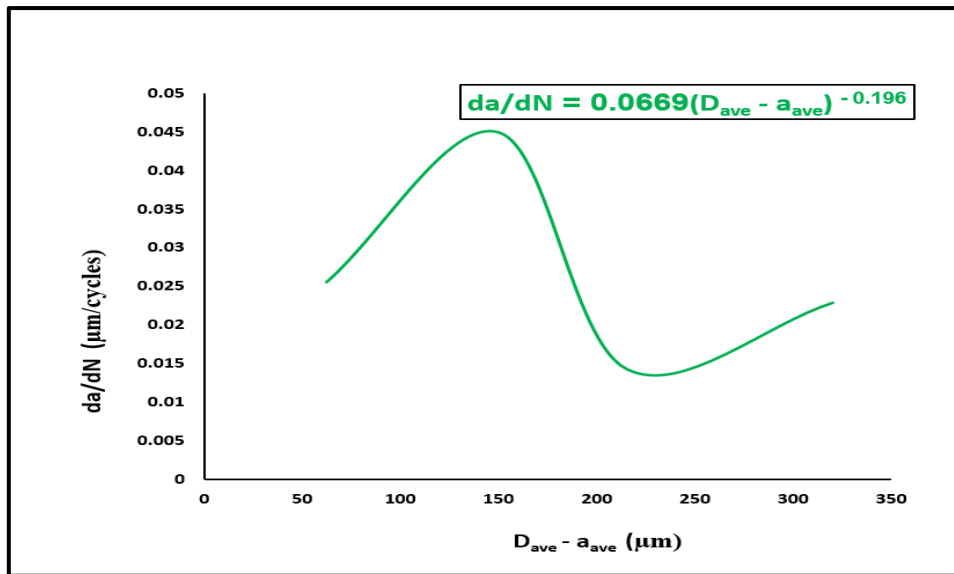


Figure 15. The short crack of AA2014

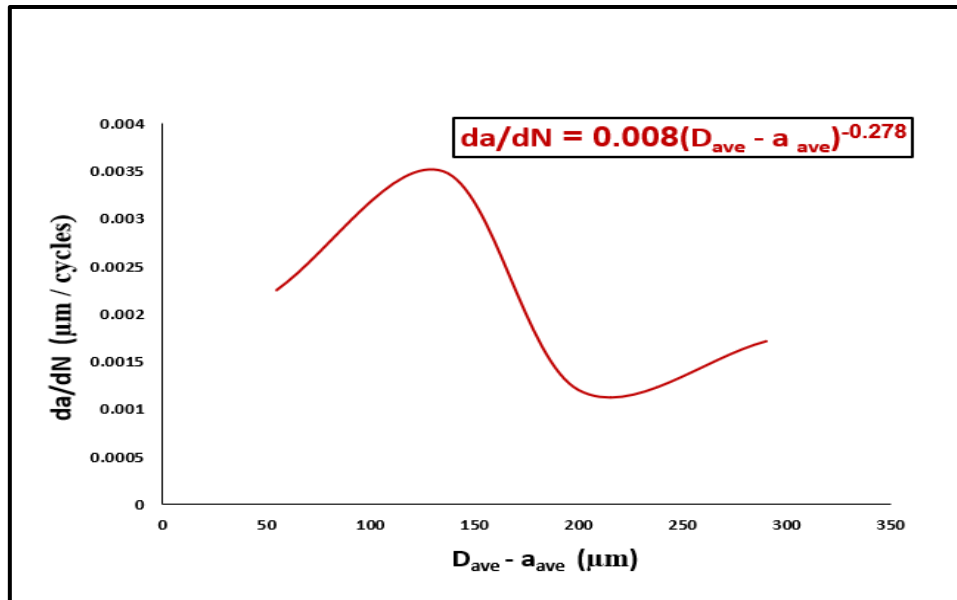


Figure 16. The short crack of AA7075-T651

The Figures 15 and 16 above show that the rate of crack speed ( $da/dN$ ) of the short cracks increases quickly and irregularly at the start of crack growth, then slows down when the average length of the crack ( $a_{ave}$ ) reaches the average grain size diameter. However, the rate of crack speed ( $da/dN$ ) becomes zero if the ( $a_{ave}$ ) is approximately equal to ( $D_{ave}$ ), because the grain boundaries represent a strong obstacle to the growth of the crack, and for a very short time, the crack growth stops [19].

The results obtained in Table 8 were used to develop two mathematical equations that explain the correlation between the average grain size diameter for both alloys and the short crack speed rate as follows:

For AA2014:

$$\frac{da}{dN} = 0.0669 (D_{ave} - a_{ave})^{-0.196} \quad (9)$$

For AA7075-T651:

$$\frac{da}{dN} = 0.008 (D_{ave} - a_{ave})^{-0.278} \quad (10)$$

To calculate the fatigue life of short cracks, equations (9) and (10) were integrated and denoted as follows:

For AA2014:

$$N_s = \frac{D_{ave}^{1.196}}{80.0124 \cdot 10^{-3}} \quad (11)$$

For AA7075-T651:

$$N_s = \frac{D_{ave}^{1.278}}{10.224 \cdot 10^{-3}} \quad (12)$$

### 3.6 Results of long cracks

It was assumed that these cracks extend from the point at which they cross the grain boundary ( $D_{ave}$ ) until they reach the critical crack length ( $a_c$ ),

at which point the material quickly fractures. Tables 6 and 7 list the long crack results for AA2014 and AA7075-T651, respectively.

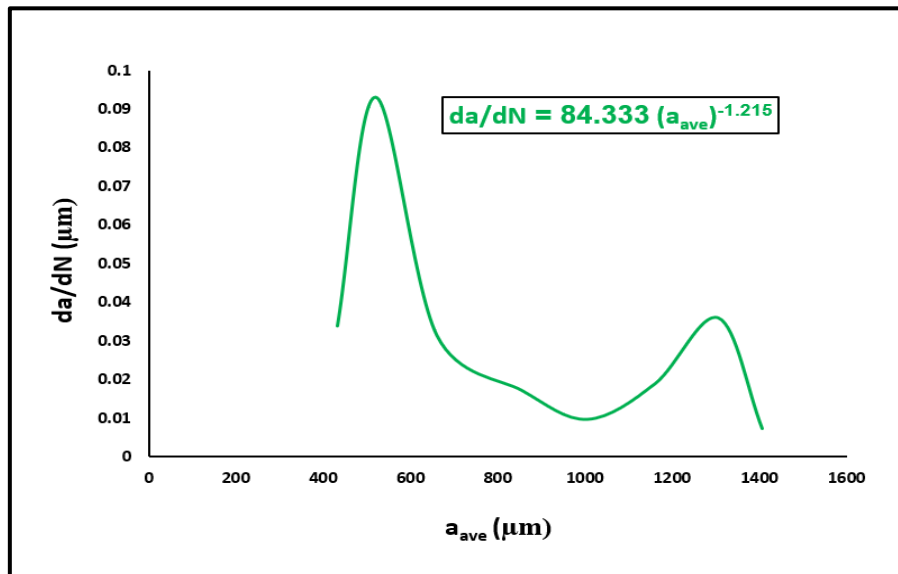


Figure 17. The long crack of AA2014

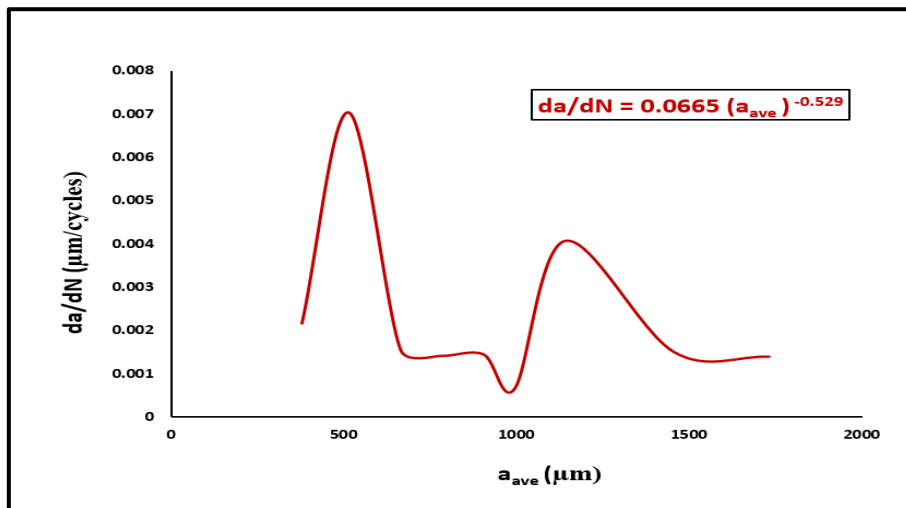


Figure 18. The long crack of AA7075-T651

The length of long cracks is unaffected by the material's microstructure, and these cracks appear when the material is subjected to high stresses, where the impact of small cracks can be disregarded. It was therefore assumed that the length of these cracks starts when they cross the grain boundary ( $D_{ave}$ ) and continues until they reach the critical crack length ( $a_c$ ), at which point the specimen unexpectedly fractures. Figures (17) and (18) describe how these cracks behave.

In order to represent the crack speed behavior of long cracks in both aluminum alloys, two mathematical equations were developed based on the findings in Tables 6 and 7, and they are presented as follows:

For AA2014:

$$\frac{da}{dN} = 84.333 (a_c)^{-1.215} \quad (13)$$

For AA7075-T651:

$$\frac{da}{dN} = 0.0665 (a_c)^{-0.529} \quad (14)$$

where  $a_c$  is the critical crack length, expressed in ( $\mu\text{m}$ ).

To calculate the fatigue life of long cracks, equations (13) and (14) were integrated. The following is how these equations are expressed:

For AA2014:

$$N_1 = \frac{a_c^{2.215} - D_{ave}^{2.215}}{186.797595} \quad (15)$$

For AA7075-T651:

$$N_1 = \frac{a_c^{1.529} - D_{ave}^{1.529}}{101.6785 * 10^{-3}} \quad (16)$$

For AA2014, the total fatigue life is:

$$N_T = N_s + N_1 \quad (17)$$

$$N_T = \frac{D_{ave}^{1.196}}{80.0124 * 10^{-3}} + \frac{a_c^{2.215} - D_{ave}^{2.215}}{186.797595} \quad (18)$$

For AA27075-T651, the total fatigue life is:

$$N_T = N_s + N_1 \quad (19)$$

$$N_T = \frac{D_{ave}^{1.278}}{10.224 * 10^{-3}} + \frac{a_c^{1.529} - D_{ave}^{1.529}}{101.6785 * 10^{-3}} \quad (20)$$

Figures 19 and 20 depict, for the aluminium alloys AA2014 and AA7075-T651, respectively, the behaviour of small and long fractures.

### 3.7 Total fatigue life estimation

The following estimates were made for the overall fatigue life of the aluminium alloys AA2014 and AA7075-T651:

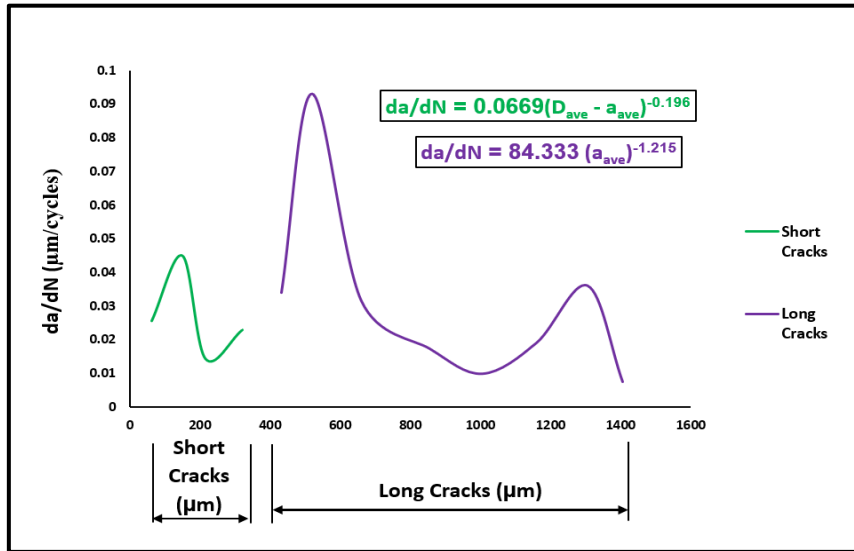


Figure 19. The short and long cracks of AA2014

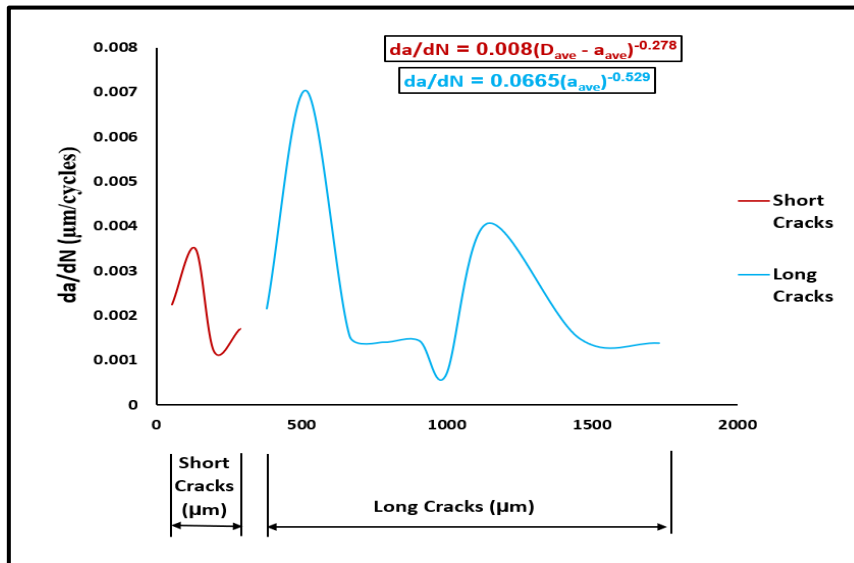


Figure 20. The short and long cracks of AA7075-T651

**Table 10:** compares the predicted crack growth model with the experimental fatigue life

AA2014			AA7075-T651		
$\sigma_p$ (MPa)	$N_{f\text{Exp}}$ (cycles)	$N_{\text{model}}$ (cycles)	$\sigma_p$ (MPa)	$N_{f\text{Exp}}$ (cycles)	$N_{\text{model}}$ (cycles)
105 (0.2UTS)	66500	63275	122 (0.2UTS)	1138000	1052964

The results listed in Table 10 were obtained from tracking cracks for one specimen of each alloy for regular time periods until the final fracture of the specimen under a given stress to model short and long fatigue cracks. Fatigue testing was also conducted on two other specimens under the same stress to calculate the fatigue life of both alloys without tracking cracks and compare the two results to prove the validity of the crack modeling.

#### 4. Conclusion

These are the major conclusions:

- 1- Short crack growth rates develop more fast than long crack growth rates do.
- 2- The short cracks are affected by the grain boundary because it creates a strong barrier to prevent the cracks from expanding.
- 3- The length of long cracks is affected by applied loads, not by the microstructure of the material.
- 4- It is successful to compute the fatigue life of both alloys under constant amplitude loads using the short and long fracture models.

#### References

- [1] Zhengheng Lian, Minjie Li and Wencong Lu. (2022). Fatigue life prediction of aluminum alloy via knowledge-based machine learning. *International Journal of Fatigue* Volume 157, April 2022, 106716, <https://doi.org/10.1016/j.ijfatigue.2021.106716>.
- [2] Anoop Kumar Pandouria and Vikrant Tiwari. (2023). Investigations into the static and dynamic fracture initiation and propagation toughness of AA2014-T6 incorporating temperatures effects. *Engineering Fracture Mechanism*. Vol.281, 28 March 2023, <https://doi.org/10.1016/j.engfracmech.2023.109130>.
- [3] Zhang J, Song B, Wei Q, Bourell D and Shi Y. (2018). A Review of Selective Laser Melting of Aluminium Alloys: Processing, Microstructure, Property and Developing Trends. *Journal of Materials Science and Technology* (2018), <https://doi.org/10.1016/j.jmst.2018.09.004>.
- [4] Susheel Dharmadhikari and Amrita Basak. (2022). Fatigue damage detection of aerospace-grade aluminium alloys using feature-based and feature-less deep neural networks. *Machine Learning with Applications* Vol. 7, 15 March 2022, <https://doi.org/10.1016/j.mlwa.2021.100247>.
- [5] Fredrik Bjørheim, Sudath C. Siriwardane and Dimitrios Pavlou. (2022). A review of fatigue damage detection and measurement techniques. *International Journal of Fatigue* Vol. 154, January 2022, <https://doi.org/10.1016/j.ijfatigue.2021.106556>.
- [6] J. K. Knotte (2023). *Fundamental of Fracture Mechanics*. First Edition, <http://www.icfweb.org>.
- [7] Haigen Jian, Jian Luo, Xianmin Tang, Xue Li and Cheng Yan (2017). Influence of microstructure on fatigue crack propagation behaviors of an aluminium alloy: role of sheet thickness. *Engineering Fracture Mechanics*, Volume 180, Pages 105-114, <https://doi.org/10.1016/j.engfracmech.2017.05.038>.
- [8] V. Chaves, G. Beretta, J.A. Balbin and A. Navarro (2019). Fatigue life and crack growth direction in 7075-T6 aluminum alloy specimens with a circular hole under biaxial loading. *International Journal of Fatigue*, Volume 125, Pages 222-236, <https://doi.org/10.1016/j.ijfatigue.2019.03.031>.
- [9] Abhay K. Singh, Siddhant Datta, Aditi Chattopadhyay, Jaret C. Riddick and Asha J. Hall (2019). Fatigue Crack Initiation and Propagation Behaviour in Al – 7075 Alloy under In-Phase Bending-Torsion Loading. *International Journal of Fatigue*, Volume 125, Pages 346-356, <https://doi.org/10.1016/j.ijfatigue.2019.05.024>.
- [10] Y. Li, D. Reirant, H. Xueb, T. Gaob and Z. Suna (2019). Fatigue properties and cracking mechanisms of a 7075-aluminum alloy under axial and torsional loadings. *Procedia Structural Integrity*, Volume 125, Pages 637-644, <https://doi.org/10.1016/j.prostr.2019.12.069>.
- [11] D.J. Bang and A. Ince (2020). Short and long crack growth model based on 2-parameter driving force and crack growth thresholds. *International Journal of Fatigue*, Volume 141, <https://doi.org/10.1016/j.ijfatigue.2020.105870>.
- [12] Rajendran Chinnasamy, Samson Jerold Samuel Chelladurai and Tushar Sonar. (2021). Investigation

- on Microstructure and Tensile Properties of High-Strength AA2014 Aluminium Alloy Welds Joined by Pulsed CMT Welding Process. *Advances in Materials Science and Engineering* Volume 2021, Article ID 8163164, 8 pages, <https://doi.org/10.1155/2021/8163164> .
- [13] E. Rendell, A. Hsiao, and J. Shirokoff. (2017). Effect of Partial Cladding Pattern of Aluminium 7075 T651 on Corrosion and Mechanical Properties. *Advances in Materials Science and Engineering* Volume 2017, Article ID 5282659, 7 pages, <https://doi.org/10.1155/2017/5282659>.
- [14] ASTM B211M Standard Specification for aluminum and aluminum alloys, round rod and bar, 2012, <https://titanium.com/astm-b211-specification> .
- [15] Xiang Li, Linyi Cui, Jikang Li, Ying Chen, Wei Han, Sara Shonkwiler and Sara McMains. (2022). Automation of intercept method for grain size measurement: A topological skeleton approach. *Materials & Design* 224 (2022) 111358, <https://doi.org/10.1016/j.matdes.2022.111358>
- [16] Robert L. and Joseph A. Untener. (2016). *Applied Strength of Materials*. Six Edition, <http://taylorandfrancis.com>.
- [17] Zahraa M. Chalooob, Hussain Jasim M. Alalkawi, Saad Theeyab Faris (2023). Crack growth model for estimation the fatigue life of AA 2142-T351 under variable loading without generating S-N curve. *Corrosion and Production* Vol.51 Issue. 1 (2023), <https://www.fsyfh.cn/view/article/2023/410.php>.
- [18] Shanqin Hou and Jinqian Xua (2018). An approach to correlate fatigue crack growth rate with S-N curve for an aluminium alloy LY12CZ. *Theoretical and Applied Fracture Mechanics*, Volume 95, June 2018, Pages 177-185, <https://doi.org/10.1016/j.tafmec.2018.02.016> .
- [19] W.B. Shou, D.Q. Yi, H.Q. Liu, C. Tang, F.H. Shen and B. Wang (2016). Effect of grain size on the fatigue crack growth behaviour of 2524-T3 aluminium alloy. Volume 16, Issue 3, May 2016, Pages 304-312, <https://doi.org/10.1016/j.acme.2016.01.004> .